

41.8-nm Xe⁸⁺ laser driven in a plasma waveguide

A. Butler, A. J. Gonsalves, C. M. McKenna, D. J. Spence, and S. M. Hooker*

*Department of Physics, University of Oxford, Clarendon Laboratory, Parks Road, Oxford OX1 3PU, United Kingdom*S. Sebban,[†] T. Mocek, and I. Betttaibi*Laboratoire d'Optique Appliquée, ENSTA/Ecole Polytechnique, CNRS UMR 7639, F-91761 Palaiseau cedex, France*B. Cros[‡]*LPGP, UMR 8578, CNRS, Université Paris XI, Bâtiment 210, 91405 Orsay, France*

(Received 19 April 2004; published 30 August 2004)

An experimental demonstration of an optical field ionization short-wavelength laser driven in a gas-filled capillary-discharge waveguide is described in detail. Guiding of high-intensity laser pulses has previously been demonstrated with this type of waveguide for capillary discharges in hydrogen. For the present experiments xenon gas was mixed with the hydrogen, and strong lasing on the $4d^95d-4d^95p$ transition in Xe⁸⁺ at 41.8 nm was observed. Under optimum conditions the short-wavelength laser output achieved with the waveguide was found to be greater than that from a Xe gas cell. Measurements of the transmission of the pump laser pulses through the waveguide show that the short-wavelength laser signal was greatest under conditions for which the pump laser pulses were well guided. Simulations of the propagation of the pump laser radiation are presented for a range of initial plasma conditions, and these indicate that the laser-plasma interaction length achieved was greatly increased compared to that which can be achieved in a gas cell.

DOI: 10.1103/PhysRevA.70.023821

PACS number(s): 42.55.Vc, 52.38.Hb

I. INTRODUCTION

In order to create a population inversion on an extreme-ultraviolet (xuv) or soft-x-ray laser transition, a large pump power density must be supplied to overcome the high rate of spontaneous decay of the upper laser level. Ever since the first demonstrations [1,2] of lasing at short wavelengths, considerable effort has been devoted to reducing the size and increasing the repetition rate of the visible pump lasers employed. Recently progress towards these goals has been made by using picosecond or femtosecond pump laser pulses of only moderate energy [3–6]. Short-pulse lasers of this type are compact and able to operate at high repetition rates, making them attractive pump sources for short-wavelength lasers. An alternative technique, in which fast electrical discharges are used to provide the pump power, has been successfully employed [7] to pump xuv lasers operating at 46 nm or longer, but it has proved difficult to scale to shorter wavelengths.

Traveling-wave excitation is often necessary when driving short-wavelength lasers owing to the brief duration of the gain. For this geometry the pump laser energy required is minimized by employing longitudinal pumping. However, with this configuration diffraction and refraction of the pump beam limit the gain length to only a few millimeters, and as a consequence the small-signal gain coefficient must be very high if lasing is to be achieved. Furthermore, the energy extraction and transverse coherence of the short-wavelength

beam are likely to be poor. A direct way to increase the interaction length would be to employ a larger focal spot, but this would greatly increase the pump laser pulse energy required. A more favorable approach is to guide the pump laser pulse over long lengths.

Several techniques for guiding high-intensity laser radiation have been investigated, including guiding in hollow capillaries [8,9], relativistic channeling [10], and several types of plasma waveguide [11–15]. However, few of these have been used to increase the gain length of short-wavelength lasers. Plasma channels formed by discharge or laser ablation of a LiF capillary have been used to demonstrate [16] recombination lasing on the $n=2 \rightarrow 1$ transition at 13.5 nm in Li²⁺. In that work lasing was achieved with 248 nm pump radiation for 5-mm-long laser-ablated capillaries and with 1053 nm pumping for 14-mm-long discharge-ablated capillaries. Janulewicz *et al.* have investigated [17] collisionally excited short-wavelength lasers driven within a plasma channel formed by a Z-pinch discharge. Those authors employed 1 ps pump pulses from a Nd:glass laser to achieve transient gain on the $3p-3s$ transition at 60.8 nm in S⁶⁺. However, in that work the spot radius of the pump laser was very large, approximately 170 μm , so that the capillary length (30 mm) was significantly less than the Rayleigh range of the pump beam. While these early results show the promise of driving short-wavelength lasers within a plasma channel, evidence for generation of gain over the full length of the waveguide has not yet been presented.

In this paper we present in detail the results of the first experimental demonstration of a short-wavelength laser driven within a gas-filled capillary-discharge waveguide. This is also the first time that a collisionally excited optical field ionization laser has been driven in any waveguide. The

*Electronic address: simon.hooker@physics.ox.ac.uk

†Electronic address: sebban@ensta.fr

‡Electronic address: brigitte.cros@pgp.u-psud.fr

results of this experiment have previously been described [18] in brief, but this present report contains additional experimental data, results of numerical simulations, and further discussion.

The paper is organized as follows. In Secs. II and III we briefly describe the gas-filled capillary-discharge waveguide and the mechanisms by which it operates, and outline the short-wavelength laser scheme investigated in the present paper. In Sec. IV the experimental layout and methods employed are described in detail, the results being described in Sec. V. Numerical simulations of the propagation of the pump laser pulse through the waveguide, under the conditions found experimentally to optimize the Xe⁸⁺ laser signal, are presented in Sec. VI. Finally the results are discussed in Sec. VII and conclusions drawn in Sec. VIII.

II. GAS-FILLED CAPILLARY-DISCHARGE WAVEGUIDE

The present work utilizes a gas-filled capillary-discharge waveguide [19]. In this type of waveguide an electrical discharge is struck along the inside of a gas-filled capillary to form a plasma waveguide. Magnetohydrodynamic (MHD) simulations [20] by Bobrova *et al.* showed that capillary discharges in H₂ form a fully ionized plasma channel with a density that increases approximately quadratically with radial distance from the axis. The channel is formed by radial heat conduction to the capillary walls, which causes the plasma temperature to be greatest, and hence the density to be lowest, near the capillary axis.

In an ideal plasma waveguide the plasma has a parabolic profile of the form $N_e(r) = N_e(0) + \Delta N_e(r/r_{ch})^2$, where $N_e(r)$ is the electron density at a distance r from the capillary axis and ΔN_e is the increase in electron density at $r = r_{ch}$ from the axial value $N_e(0)$. An intense laser pulse passing through a plasma experiences a refractive index which is dominated by the contribution of free electrons in the plasma and is given by $n = \sqrt{1 - N_e e^2 / (m_e \epsilon_0 \omega^2)}$, where ω is the angular frequency of the laser radiation and relativistic effects have been neglected. It follows that in a parabolic plasma channel the refractive index is peaked on axis and acts to counter diffraction and ionization-induced defocusing of a laser pulse. If no further ionization of the plasma occurs and ponderomotive and relativistic effects are negligible, a Gaussian beam will propagate [21] along a parabolic channel with a constant spot radius W_M , provided $W_M = [r_{ch}^2 / (\pi r_e \Delta N_e)]^{1/4}$, where r_e is the classical electron radius. If the spot radius is not matched to W_M , then the laser spot radius oscillates as the pulse travels along the capillary. This mismatch may be characterized by the parameter $N = W_M / W_i$. In this case the spot radius varies between the spot radius at injection into the capillary (W_i) and $N^2 W_i = W_M^2 / W_i$, with a length period given by $\pi^2 W_M^2 / \lambda = \pi Z_{RM}$, where Z_{RM} is the Rayleigh range corresponding to a laser spot of spot radius W_M . This intensity oscillation will not be particularly severe for a small spot radius mismatch.

Guiding high-intensity laser pulses

In earlier work we demonstrated [22,23] low-loss guiding of laser pulses with a peak input intensity of up to 1.2

$\times 10^{17}$ W cm⁻², over lengths of up to 50 mm through H₂-filled capillary-discharge waveguides.

In order to demonstrate short-wavelength lasing in a waveguide of this type, the H₂ gas fill must be doped with the lasant gas. Of course, if the concentration of the lasant gas is too high, the optical field ionization—which is required to generate and pump the lasant ion—will contribute a high electron density near the axis, destroying the plasma channel and preventing a long interaction length from being achieved.

III. SHORT-WAVELENGTH LASER SCHEME

For pump laser intensities of order 10¹⁶ W cm⁻² the electric field of the radiation is comparable to the intra-atomic field experienced by bound electrons in atoms and ions. As a consequence the bound electrons are rapidly ionized owing to gross distortion of the intra-atomic potential, a process known as optical field ionization (OFI). The rate of OFI exhibits a thresholdlike behavior with the laser intensity, the threshold intensity corresponding to that which just removes the barrier formed by the sum of the intra-atomic and laser potentials [24]. The threshold nature of OFI makes it an attractive mechanism for generating plasmas suitable as gain media for short-wavelength lasers since the ion stage generated may be controlled by adjusting the laser intensity. Further, the energy of the electrons after the passage of the laser pulse can be controlled through the polarization of the laser radiation: linear polarization generates relatively cold electrons, suitable for pumping recombination lasers; circular polarization produces hot electrons which can pump population inversions by electron collisions [25].

For this proof-of-principle experiment it was decided to investigate the collisionally excited OFI laser scheme in Xe⁸⁺ proposed [26], and later demonstrated [5], by Lemoff *et al.* In the past few years Sebban *et al.* have characterized the operation of this laser in detail and reported saturation of the laser transition [27–29]. In both these previous experiments femtosecond laser pulses were focused into a differentially pumped gas cell containing pure Xe, and the gain length achieved was less than 8.5 mm, owing to diffractive and refractive defocusing of the pump beam.

The Xe⁸⁺ laser operates as follows. Gaseous Xe is ionized to Xe⁸⁺ by OFI with high-intensity, circularly polarized radiation from a Ti:sapphire laser. The threshold pump laser intensity for forming Xe⁸⁺ is approximately 5×10^{16} W cm⁻². Achieving the correct laser intensity on target is vital to forming the required ion stage for the laser system. For example, the threshold intensity to overionize to form Xe⁹⁺ is 2×10^{17} W cm⁻², only about 4 times the intensity necessary to form Xe⁸⁺. The use of circularly polarized radiation ensures that the field-ionized electrons retain high energies after passage of the pump laser pulse, thereby allowing rapid collisional excitation of the upper laser level.

A simplified diagram of the atomic structure of Xe⁸⁺ is shown in Fig. 1. This shows the dominant collisional pumping and deexcitation routes, and some important electromagnetic transitions. The laser transition is $4d^9 5d^1 S_0 - 4d^9 5p^1 P_1$ at 41.81 nm.

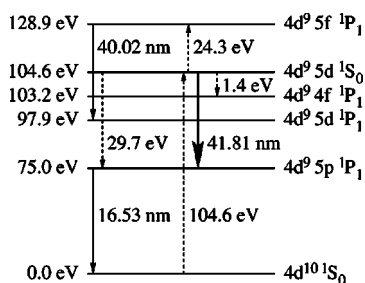


FIG. 1. Partial energy level diagram of Xe⁸⁺ showing the laser line at 41.81 nm. The dashed lines show the dominant collisional excitation and deexcitation routes for the upper laser level. The figure is adapted from those given in work [5,26] by Lemoff *et al.*

IV. APPARATUS

The experiments described in this paper were conducted at the Laboratoire d'Optique Appliquée (LOA), part of the Ecole Normale Supérieure de Techniques Avancées (ENSTA). The pump laser employed in the present experiments was a 3-J Ti:sapphire laser [30] with a central wavelength of 820 nm. The laser system employs only multipass amplifiers, rather than regenerative amplifiers, in order to minimize prepulses to the main laser pulse. For the present experiments the pulse duration was measured to be 37 fs full width at half maximum (FWHM) (assuming a Gaussian temporal profile), and the energy available on target was up to 300 mJ.

A. Experimental layout

The experimental arrangement employed is shown in Fig. 2. Radiation from the Ti:sapphire laser was circularly polarized by a quarter-wave plate and focused into the entrance of the capillary waveguide by an off-axis paraboloid (not shown) used at $f/25$. The radiation transmitted by the capillary was reduced in intensity by reflections from three wedged optical flats (W1–W3) and then rendered parallel by a lens (L1) of focal length 1 m. The beam was refocused by

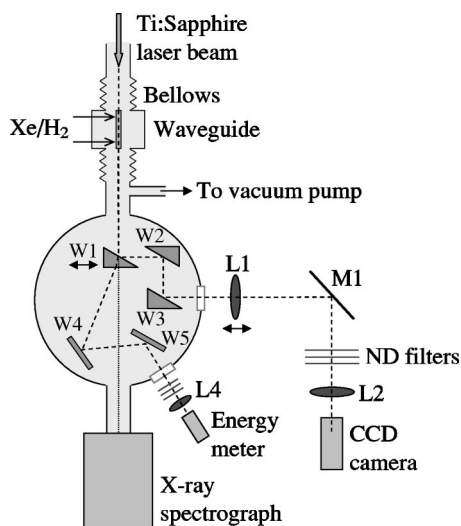


FIG. 2. Schematic diagram of the experimental layout employed.

a lens (L2) of focal length 300 mm and imaged onto a 12-bit charge-coupled-device (CCD) camera by a 20× microscope objective. The overall magnification of this imaging system was 3.5. The resolution was limited by the aperture of the vacuum chamber window and W1 such that L1 was effectively $f/25$.

Radiation transmitted by W1 was reduced in intensity by reflection from the surfaces of W4 and W5 and loosely focused by lens L4 onto the surface of a large area pyroelectric energy meter to provide a measurement of the transmitted pulse energy. The energy of the laser pulses entering the capillary was determined by a photodiode (not shown), located prior to the paraboloid. The signal from the photodiode was calibrated to the absolute energy on target. The energy transmission of the waveguide was then determined by comparing the measured input and transmitted energies with those recorded when the capillary was replaced by an evacuated beam pipe.

The CCD camera recorded beam profiles of the pump laser radiation transmitted by the capillary. These were converted to transverse fluence profiles using the measured energy of the transmitted radiation and the measured magnification of the imaging system. Since a partially ionized plasma target is expected to distort the temporal profile of the transmitted laser pulses, fluence, rather than intensity, profiles are presented.

The pump laser fluence profile at the input of the capillary was measured by adjusting the imaging system to image the entrance plane of the capillary and replacing the capillary by an evacuated beam pipe. The energy transmission T_E was calculated from the measured values for the transmitted and input laser pulse energies. The fluence transmission T_F was calculated similarly from the peak of the transmitted fluence profile and the peak of the input fluence profile scaled by the measured input energy of each laser shot.

The mean energy of the laser pulses input to the capillary during the experiments was (240 ± 20) mJ, and the beam focus was measured to have a peak fluence of 9.8×10^3 J cm⁻², corresponding to a peak input intensity of 2.5×10^{17} W cm⁻². Fitting a Gaussian intensity profile of the form $I(r) = I(0)e^{-2(r/W)^2}$ yields a spot radius W of approximately 34 μm, corresponding to a Rayleigh range of 4.4 mm for a diffraction-limited Gaussian beam. In practice the Rayleigh range will have been shorter than this owing to aberrations on the beam.

The spectrum of the xuv radiation leaving the capillary was recorded by moving W1 so as to allow the radiation to enter an x-ray spectrograph, the pump laser radiation being blocked by a 0.3-μm-thick Al filter. The x-ray spectrograph [29] utilized a 2000-lines/mm transmission grating to disperse the spectrum from the zero order up to ≈ 70 nm onto a 16-bit x-ray CCD camera.

B. Waveguide design

The capillary waveguide design employed in the present experiments was similar to that described previously [23]. The electrical discharge path ran between earth electrodes located at the ends of the capillary and a central high-voltage electrode.

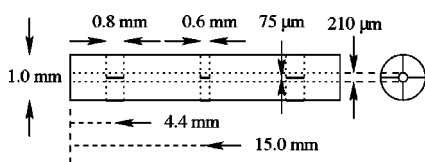


FIG. 3. 30-mm-long capillary design. The capillary is shown in plan and end view. The dotted lines indicate internal structure and the dashed lines are guides to the eye.

The electric circuit which generated the discharge pulse was similar to that described [22] previously. A 4.5-nF storage capacitor was charged to 20–30 kV and switched across the capillary using a thyratron switch. The circuit inductance was increased from that employed in previous work [23] to slow the discharge and reduce the peak current. The current pulse produced was measured with a Rogowski coil and was found to be a damped, approximately sinusoidal profile, with a quarter period of 500 ns and a peak value of 105 A per arm (temporal behavior as shown in Fig. 5). The time at which the laser pulse was injected into the capillary was determined by detecting with a photodiode the radiation leaking through a mirror located a known distance before the capillary. The injection time delay t is defined from the initiation of the measured discharge current pulse.

Alumina (Al_2O_3) capillaries of length 30 mm and internal diameter 210 μm , of the design shown in Fig. 3, were employed. In order to introduce gas into the capillary, slots of length 0.8 mm and approximately 75 μm wide were machined with their centers located 4.4 mm from the ends of the capillary. To increase the gas flow rate, four slots were drilled, with azimuthal symmetry, near both ends of the capillary. Four central, 0.6-mm-long slots, were also machined with azimuthal symmetry, to allow the discharge current to flow.

The capillary and electrodes were mounted in a holder [23] which was connected to the surrounding vacuum system by flexible bellows. The entire system was mounted on a five-axis optical stage to enable alignment of the axis of the capillary to the input laser beam.

Premade mixtures of Xe and H_2 gas were flowed into the capillary, the flow rate of the gas mix being measured by a gap flow meter calibrated in separate experiments against the pressure at the center of the capillary.

In order to facilitate a comparison with previous demonstrations of lasing on this transition, xuv lasing in a Xe-filled gas cell similar to that used by Sebban *et al.* was also investigated. For those experiments the waveguide was removed and the cell positioned so that the vacuum focus of the pump laser was located 2.5 mm after the entrance pinhole. In this configuration the pump laser radiation entered and exited the gas cell through two pinholes of 200–500 μm diameter, separated by 4 mm. These values for the cell length and laser focal position are very similar to those found [29] to be optimum by Sebban *et al.*

V. RESULTS

A. Short-wavelength lasing

Lasing on the 41.8-nm transition of Xe^{8+} was investigated for a wide range of Xe/H mixtures, total gas pressure, and

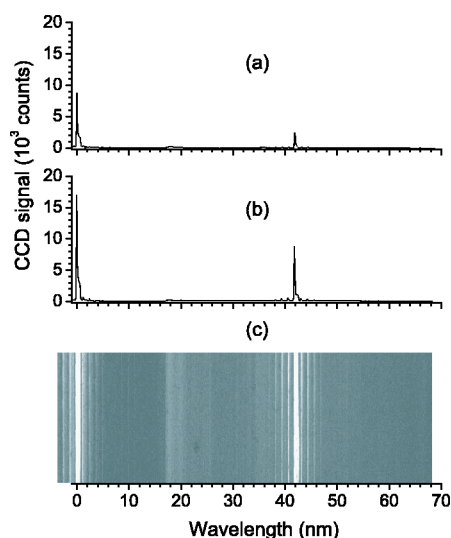


FIG. 4. xuv spectra, integrated over ten pump laser shots, at the optimum gas conditions for (a) the gas cell, and (b) a 30-mm-long capillary. In (c) the raw CCD image of the spectrum recorded the waveguide is presented.

pump laser injection delay t . Lasing was first observed using a 1:7 Xe:H atom ratio gas mixture, was strongest for a mixture of 1:3, and was also observed for a mixture of 1:1.3. For the best gas mixture, the optimum total gas pressure was found to be 120 mbar.

Figure 4 shows the recorded xuv spectra integrated over ten pump laser pulses for (a) a gas cell containing 20 mbar of pure Xe and (b) a 30-mm-long gas-filled capillary-discharge waveguide with a 1:3 Xe:H atom gas mixture, a gas pressure of 120 mbar, and a delay t of 1000 ns. For both targets these conditions are those which optimized the Xe^{8+} laser signal. Figure 4(c) shows the raw CCD image obtained with the waveguide. This image has been deliberately saturated so that some features other than the zero order and laser line are visible. For example, the aluminum L edge at 17.1 nm from transmission by the filter is visible in first and second order. In some CCD images the aluminum L edge was seen up to third order and was used for calibration of the spectrometer. Note that the sharp lines either side of the zeroth-order peak at 0 nm and the x-ray laser peak arose from diffraction by the support mesh of the transmission grating.

The only spectral line which was observed in the spectrum from the gas cell or capillary was that from the Xe^{8+} laser line. The data show that strong lasing occurred at 41.8 nm for both the gas cell and waveguide, the signal from the waveguide being approximately 4 times larger.

For the optimum gas mixture of 1:3 Xe:H atoms, the Xe^{8+} laser output was found to be greatest for a total gas pressure of approximately 120 mbar, corresponding to a Xe partial pressure of approximately 50 mbar. The short-wavelength laser output was quite sensitive to the gas pressure: the full width at half maximum of the variation of the laser signal with the Xe partial pressure being approximately 20 mbar.

The shot-to-shot variation of the Xe^{8+} laser signal was also investigated by recording spectra, integrated over three pump laser shots, for five consecutive groups of shots. For these sets of three-shot spectra the Xe^{8+} laser signal varied

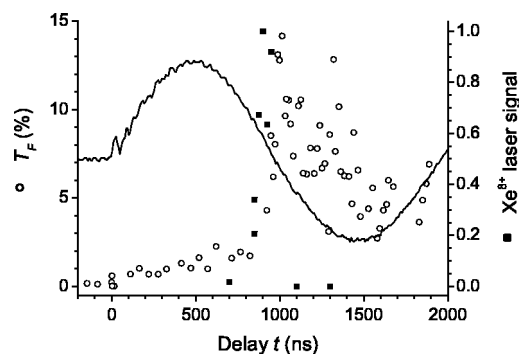


FIG. 5. The time dependence of the xuv laser signal (squares) and that of T_F (circles) during the discharge pulse. The short-wavelength laser signal is normalized to the peak value. The 30-mm-long capillary was filled with the optimum gas mixture and pressure for short-wavelength lasing. The temporal profile of the discharge current pulse is also shown.

by only 4%, indicating that short-wavelength lasing occurred on each pump laser shot.

B. Guiding

In order to understand the correlation between the experimental conditions which optimized the output of the Xe⁸⁺ laser and the behavior of the plasma channel as a waveguide, the temporal behavior of the pump laser pulse transmission was recorded for Xe/H mixtures and pure H₂ gas fills.

Figure 5 shows, for the optimum Xe⁸⁺ laser gas mixture and pressure, the dependence of the peak transmitted pump laser fluence T_F on the injection delay t of the pump laser pulses. The quantity T_F is plotted here, rather than the pulse energy transmission T_E , since it is more closely related to the OFI rate. It is seen that the fluence transmission was approximately 0.2% for laser pulses injected before the initiation of the discharge current. T_F increased slowly to around 2% for delays of approximately 900 ns. Thereafter T_F increased rapidly by a factor of approximately 6 and peaked at 13% for delays close to 1000 ns. At later times T_F fell slowly. The pulse energy transmission (T_E) behaved similarly, reaching a peak of approximately 55% for delays close to 1000 ns. The rapid rise in T_F was proportionally greater than that in T_E because there was an associated reduction in the spot radius of the guided pump laser pulse.

Figure 5 also shows, again for the optimum gas mixture, the variation of the Xe⁸⁺ laser signal with the delay t between the onset of the discharge current and the injection of the pump laser pulse. It is seen that the Xe⁸⁺ laser signal was very sensitive to the delay at which the pump laser pulse was injected. For all the experiments performed, lasing was only observed for a range of delays approximately 200 ns wide, centered at a delay of approximately 1000 ns. This correlates well with the delay t for which the highest values of T_F were observed.

Figure 6 shows the measured pulse transmission T_E and T_F for a 1:3 Xe:H atom mixture and various total gas pressures. It is seen that for all the Xe-H mixtures T_E and T_F increased relatively slowly during the first part of the dis-

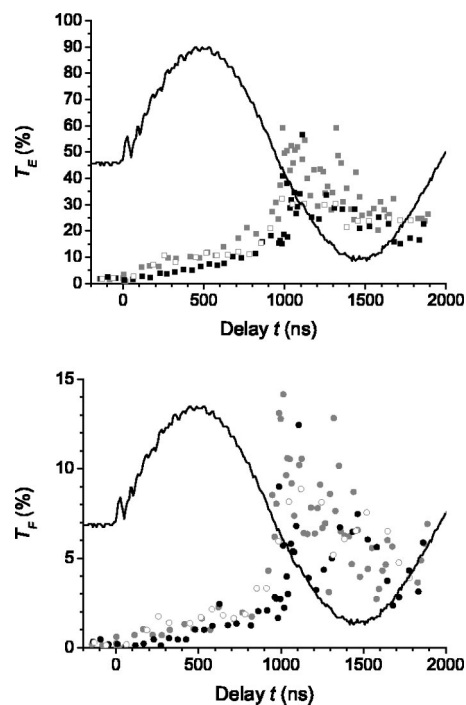


FIG. 6. Pump laser transmission through a 30-mm-long capillary, expressed as T_E and T_F , as a function of injection delay t . The capillary contained a 1:3 Xe:H atom gas mixture. The total pressure within the capillary was 90 mbar for the open symbols, 120 mbar for the gray symbols, and 180 mbar for the black symbols. The temporal profile of the discharge current pulse is also shown.

charge pulse, followed by a rapid increase at a delay close to 900 ns. The highest T_E values of around 55% were obtained for delays t of approximately 1000 ns. Thereafter T_E fell to 20% for delays t of around 2000 ns. T_F is seen to behave similarly to T_E , but as in Fig. 5 the increase in T_F was sharper than that of T_E due to the associated spatial constraint of the laser pulse for delays t close to 1000 ns. Careful inspection shows that the best guiding occurred for a total pressure of 120 mbar, equal to the total pressure that optimized the short-wavelength laser output.

The rise in T_E and T_F observed for Xe-H mixtures was much slower than previously found for capillary discharges in pure hydrogen [23]. Measurements with the present apparatus confirmed this: for discharges through capillaries filled with pure hydrogen at an initial pressure of 110 mbar T_E was found to reach 70% for delays of only 100 ns.

Figure 7 shows transverse fluence profiles of the pump laser radiation at the optimum Xe-H gas mixture and pressure for producing xuv lasing. Plots are shown for the entrance and exit plane of a 30-mm-long capillary for various delays t . It is seen that for delays $t < 0$ ns the transmitted fluence was very low. Even for a delay t as long as 823 ns the transmitted fluence was still below 2% of the peak input fluence due to the energy transmission being low and the energy which was transmitted being spread over a large area. At a delay t of 1014 ns the peak transmitted fluence was

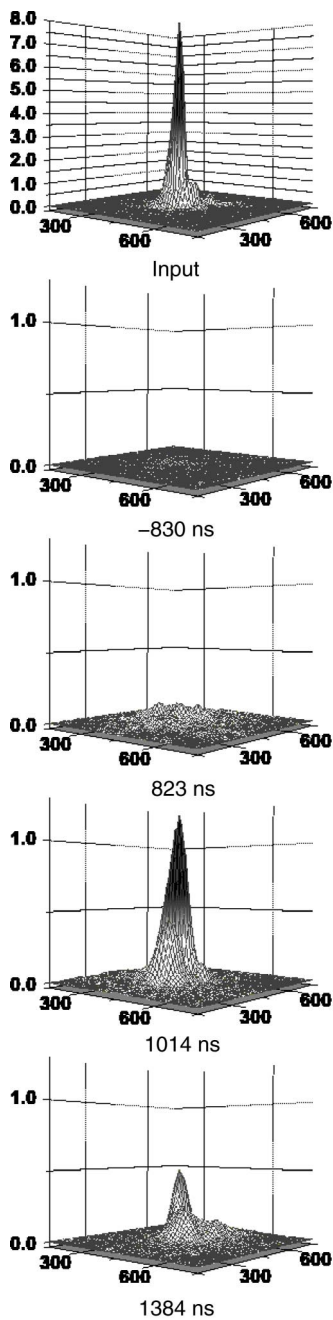


FIG. 7. Transverse fluence profiles of the pump laser radiation. The figure shows, for various delays t , the radiation at the entrance and exit plane of a 30-mm-long capillary initially filled with a 1:3 Xe:H atom gas mixture at a total pressure of 120 mbar. For all plots the spatial scale is in μm and the vertical scale is in units of kJ cm^{-2} . Note the different vertical scale for the input profile.

highest at 14% of the peak input fluence: the energy transmission had been increased and the laser radiation constrained to a spot radius of $\approx 70 \mu\text{m}$ —significantly larger than the expected matched spot size of the plasma channel, indicating that significant defocusing occurred through ionization of the Xe in the plasma channel. The decreased peak fluence observed at $t=1384 \text{ ns}$ arises primarily from a further increase in the spot radius of the transmitted laser radiation;

the energy transmission was only a little lower than that recorded for delays close to 1000 ns.

VI. NUMERICAL SIMULATIONS

In order to model the behavior of the pump laser pulses inside the waveguide, and hence determine the extent of the gain region formed by the pumping, it is necessary to know the properties of the plasma established by the capillary discharge. Unfortunately this is a complex matter, and a detailed calculation is beyond the scope of the present paper. It is possible, however, to establish reasonable ranges for the main parameters of interest.

The plasma temperature may be estimated from the MHD simulations [20] of Bobrova *et al.* That work concerns plasma waveguides formed by striking a single-ended discharge through capillaries of internal diameter $300 \mu\text{m}$ and initially filled with 67 mbar of pure H_2 gas. The electrical discharge current was taken to have a damped sinusoidal profile with a peak of 250 A and a half period of 200 ns. These conditions correspond to those used in measurements [31] of the electron density profile of the plasma channel. For those conditions it was calculated that the plasma temperature reached a maximum of 7 eV in the region of the capillary axis at the peak of the discharge current pulse.

Those MHD simulations show that for $t \geq 80 \text{ ns}$ a quasi-thermal equilibrium was established in which the Ohmic heating of the plasma was balanced by heat conduction to the capillary wall by free electrons. For these quasithermal equilibrium conditions the plasma temperature on axis was found to be given by

$$T(0) [\text{eV}] \approx 5.7 \left(\frac{I [\text{kA}]}{R_0 [\text{mm}]} \right)^{2/5}, \quad (1)$$

where I is the discharge current and R_0 the capillary radius. From this equation we calculate a plasma temperature of 5.7 eV for 210- μm -diam capillaries filled with pure H_2 gas and a peak discharge current of 105 A.

Of course, the presence of the Xe in the discharge will affect the temperature which is reached. In particular, the electrical and thermal conductivities of the plasma are expected to be reduced as approximately $1/Z$, where Z is the mean ion charge [32]. Hence the presence of the Xe ions is likely to cause greater heating of the plasma while also reducing the conductivity to the capillary walls, leading to a higher plasma temperature. We estimate, therefore, that the temperature of the plasma established by the discharge in the Xe-H gas mixtures employed in the short-wavelength lasing experiments described here is likely to be in the range 6–12 eV.

Under these conditions of temperature and density the plasma will not be in local thermodynamic equilibrium (LTE). As such the Saha equation cannot be used to calculate the mean ionization of the plasma species, although it can establish an upper limit on the ionization. We employed a numerical simulation code [33] designed specifically to model Ar-H mixtures in non-LTE conditions. By comparing

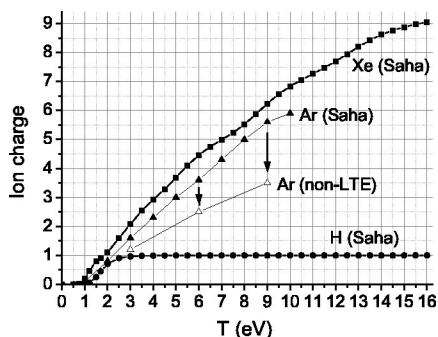


FIG. 8. Solution of the Saha equation, as a function of plasma temperature, for the degree of ionization of Ar (triangles), Xe (squares), and H (circles) for Ar-H and Xe-H mixtures. The gas mixture is that employed in the short-wavelength lasing experiments. The graph also shows the results for the equivalent Ar-H mixture calculated using a non-LTE simulation code.

the results from this code with solutions to the Saha equation for Ar-H and Xe-H mixtures, we may estimate the Xe ionization reached in the plasma. Figure 8 shows the mean ionization of H and Xe calculated from the Saha equation as a function of plasma temperature for a 1:3 Xe:H ion plasma mixture at a total ion density of $4.8 \times 10^{18} \text{ cm}^{-3}$, corresponding to 120 mbar at room temperature. The graph also shows the solutions to the Saha equation for a comparable mixture of Ar-H together with the results of the non-LTE simulation code.

Comparison of the solution to the Saha equation with the results of the non-LTE code suggests that for Ar-H mixtures the Saha equation overestimates the Ar ionization by between 1+ and 2+. Assuming that the Saha calculations for Xe overestimate the Xe ionization by a similar amount and with a similar temperature dependence, we estimate that for the range of plasma temperatures established above Xe would have been ionized to between Xe³⁺ and Xe⁷⁺. Clearly there remain significant uncertainties in the temperature and constitution of the plasma channel formed by the discharge in capillaries filled with mixtures of xenon and hydrogen, and further numerical work would be desirable. However, the range of parameters established allow us to make some progress in modeling the propagation of the pump pulses through the plasma.

Bobrova *et al.* calculated [20] that for H₂-filled capillary-discharge waveguides, the matched spot radius W_M of the plasma channel is given by

$$W_M [\mu\text{m}] \approx 1.48 \times 10^5 \frac{\sqrt{R_0} [\mu\text{m}]}{(z^* n_{i0} [\text{cm}^{-3}])^{1/4}}, \quad (2)$$

where z^* is the mean ionization of the plasma and n_{i0} the initial ion density. We have measured [31] the matched spot radius for a single-armed H₂-filled capillary-discharge waveguide to be $37.5 \mu\text{m}$ for $R_0 = 150 \mu\text{m}$ and $z^* n_{i0} = 3.3 \times 10^{18} \text{ cm}^{-3}$. We therefore take the constant of proportionality in Eq. (2) to be 1.31×10^5 , rather than the value of 1.48×10^5 calculated theoretically by Bobrova *et al.*

We may estimate W_M for Xe-H mixtures by neglecting any effect of the presence of Xe and simply making the

substitution $z^* n_{i0} \rightarrow \bar{n}_e$, where \bar{n}_e is the initial electron density of the Xe-H mixture. For example, for a mean initial Xe ionization of Xe⁵⁺ in a mixture of 1:3 Xe:H atoms, at an initial total pressure of 120 mbar, the initial ion density is $4.8 \times 10^{18} \text{ cm}^{-3}$ and the mean ionization is +2, giving a calculated matched spot radius of $24 \mu\text{m}$.

A numerical simulation code [34] was used to calculate the distribution and ionization of Xe ions after the passage of the pump laser pulse through both the gas cell and the waveguide. Figure 9 shows the calculated Xe ionization following the passage of the driving laser pulse through (a) a gas cell and (b)–(f) a plasma channel for the experimental conditions of Fig. 4 and for various degrees of preionization of the Xe. The laser pulse propagates in the positive z direction from the capillary or gas cell entrance, which is taken to be located at 0 mm. For all plots the pump laser pulse was assumed to be Gaussian with a peak intensity of $2.5 \times 10^{17} \text{ W cm}^{-2}$, a spot radius of $34 \mu\text{m}$, and full width at half maximum duration of 37 fs. The focus of the laser was positioned so that in vacuum it would have been located 2.5 mm into the gas cell and at the capillary entrance, respectively, corresponding to the experimental conditions employed. It is seen that for both the gas cell and waveguide the Xe is overionized in several regions near the axis and that therefore the longest lengths of Xe⁸⁺ occur in an annular region. For the gas cell it is calculated that Xe⁸⁺ would be generated over a length of only 4.7 mm. This may be compared to the optimum gas cell length of 4 mm found by Sebban *et al.* in experiments using the same focusing geometry, but with the vacuum focus located 1 mm into the gas cell, rather than the 2.5 mm employed here.

In contrast the results for the waveguide show that for the range of pre-ionization of Xe expected, significant lengths of Xe⁸⁺ would be formed. The length of the annular region of Xe⁸⁺ generated is seen to increase with the degree of Xe pre-ionization, ranging from approximately 10 mm for Xe³⁺ to over 60 mm for Xe⁷⁺, and reflecting the improved propagation of the driving laser pulse. The reasons for this are twofold. First, there is less additional ionization produced by the laser pulse to disrupt the guiding profile. Second, the higher initial electron density produced by the discharge reduces the matched spot size because a steeper channel is produced. This steeper channel is better able to counteract refractive defocusing arising from OFI of the Xe ions.

VII. DISCUSSION

We now discuss the implications of our results in more detail. The results show clearly that strong lasing was observed on the $4d^9 5d-4d^9 5p$ transition in Xe⁸⁺ at 41.8 nm. The strength of the short-wavelength laser signal was found to depend very critically on the delay between the onset of the discharge pulse and the injection of the pump pulse, and also to depend strongly on the pressure and constitution of the gas mixture. Furthermore, the conditions for which lasing was strongest correspond closely to those found to optimize guiding of the pump laser pulses through Xe-H mixtures. As such we conclude that lasing in Xe⁸⁺ depended not only on the plasma conditions established by the discharge, but also

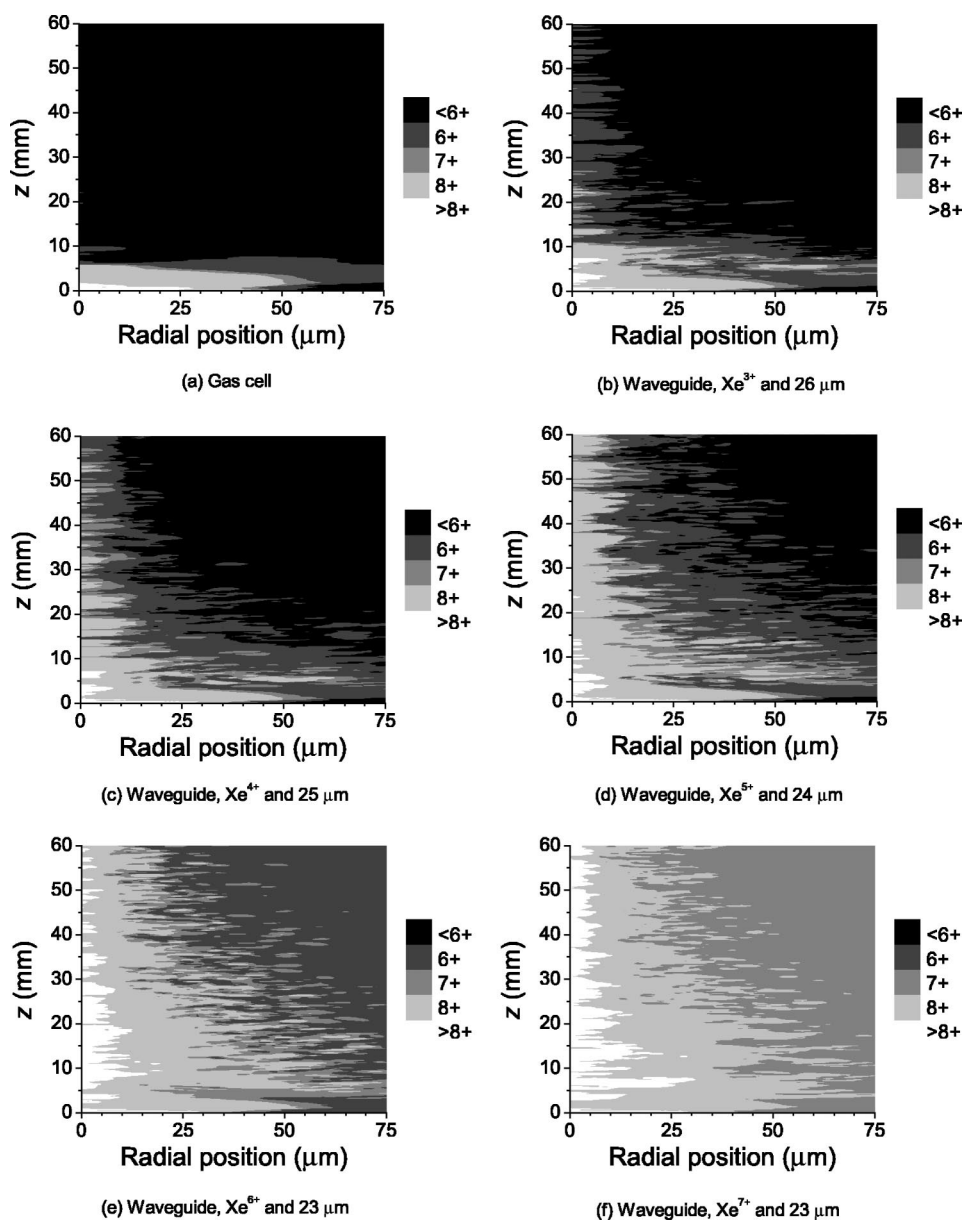


FIG. 9. The results of numerical simulations to calculate the Xe ionization after the passage of the pump laser pulse through (a) a gas cell and (b)–(f) the waveguide with various degrees of Xe pre-ionization. The gas cell is assumed to contain neutral Xe gas at a pressure of 20 mbar. The capillary is taken to be filled with 120 mbar of a 1:3 Xe:H atom gas mixture. For the capillary waveguide the degree of pre-ionization of the Xe by the discharge current and the matched spot radius are given for each graph.

on good guiding of the pump pulses through the capillary.

The guiding observed in the present experiment with Xe-H-filled capillary discharge waveguides is significantly different from that which we have previously observed with H-filled capillaries. In particular T_E and T_F were found to rise much more slowly for Xe-H-filled capillaries than those filled with pure hydrogen. The partial pressure of Xe required to observe lasing is relatively high, such that optical field ionization of the Xe will lead to strong defocusing of the propagating laser pulse. Consequently, it is necessary for the discharge to ionize the Xe to some degree before significant transmission of the pump laser pulse can occur. The observed slow rise in T_E and T_F is likely to correspond to a gradual improvement in the laser pulse transmission as the discharge heats and ionizes the Xe.

Although the Xe⁸⁺ laser signal was correlated with guiding of the pump laser, it did not follow the pump laser pulse transmission in detail since the Xe⁸⁺ laser signal reached a peak close to that in the transmission, but then fell rapidly even though T_E and T_F remained relatively high. This behavior may be due to the discharge overionizing the Xe, which would reduce or even prevent gain on the Xe⁸⁺ laser transition, or ejection of plasma from the capillary, which could reduce the gain through a lowering of the plasma density. Either of these mechanisms could prevent short-wavelength lasing from occurring while allowing good transmission of the pump laser radiation.

We also note that the observed rapid increase in T_E and T_F occurred close to the zero in discharge current. In previous work with H₂-filled capillary-discharge waveguides of the

design employed here, T_E was found to decrease slightly for delays close to a zero in the discharge current [23]. Correlations between the transmission of the waveguide, short-wavelength laser output, and zeros in the discharge current may be caused by nonuniformities in the plasma near the central electrode when the discharge current flows, but these points of detail require further investigation. They do not, however, contradict the main conclusion that good guiding of the pump laser pulse was required for lasing in Xe⁸⁺ to be observed.

The data presented in Fig. 7 show that with the optimum Xe-H gas mixture for Xe⁸⁺ lasing, the spot radius of the transmitted laser pulse at the delay for best guiding was approximately 70 μm , significantly bigger than either that of the input pulse or the expected matched spot radius of the plasma channel. At a radius equal to that of the capillary wall, a lowest-order Gaussian beam with a spot radius of 70 μm has an intensity equal to 1% of that on axis. As such, guiding of the pump laser pulses may have been affected, to some extent, by interactions with the capillary wall. However, the strong dependence on the delay t of the energy and spatial profile of the transmitted laser pulses indicates that the guiding was dominated by the plasma channel; if the role of the plasma channel was small compared to that of reflections from the capillary wall, the energy and spatial profile of the transmitted pulse would be essentially independent of t once the discharge had sufficiently ionized the Xe to allow guiding. We note that in the simulations presented here, radiation reaching the capillary wall was absorbed and hence reflections from the wall were eliminated. The inclusion of reflection of pump laser radiation at the capillary wall would refocus energy towards the capillary axis and tend to increase the length of Xe⁸⁺ produced under otherwise identical conditions.

Although the simulations show that the length over which Xe⁸⁺ is formed is increased by the use of a Xe-H-filled capillary-discharge waveguide, the kinetics of the short-wavelength laser transition will be different from those in a gas cell [19]. In particular the small-signal gain coefficient is likely to be reduced by a combination of reduction of the population inversion owing to increased collisional deexcitation of the upper laser level, increased Doppler and Stark

widths of the laser transition due to the higher ion temperature and the increased electron density in the plasma, reduced pumping of the upper laser level since there will be fewer hot OFI electrons following preionization of the Xe by the discharge, and possible cooling of the OFI electrons by collisions with the relatively cold electrons formed by the discharge. A detailed calculation of the kinetics of the Xe⁸⁺ laser operating under the conditions found in the waveguide plasma channel is beyond the scope of the present paper. However, the facts that lasing was observed with the capillary-discharge waveguide and the signal was at least as strong as that from the gas cell imply that for the present experiments the increase in gain length more than compensated any decrease in small-signal gain. Further, we note that the presence of a dense pool of cold electrons in the plasma waveguide could significantly enhance the small-signal gain coefficient of recombination lasers driven within gas-filled capillary-discharge waveguides [35].

VIII. CONCLUSIONS

In summary, we have presented in detail the results and analysis of an experiment to demonstrate lasing on an extreme ultraviolet transition driven in a gas-filled capillary-discharge waveguide. Analysis shows that lasing was strongly correlated with good guiding of the pump pulse, and numerical simulations indicate that gain is likely to have been achieved over a significant fraction of the 30 mm length of the capillary. The success of this proof-of-principle experiment suggests that this and other short-wavelength lasers could be driven within waveguides of this type, leading to increased energy output and reduced beam divergence.

ACKNOWLEDGMENTS

The authors acknowledge invaluable technical assistance from the laser support staff at Laboratoire d'Optique Appliquée-ENSTA. A.B., A.J.G., and C.M.Mc.K. are grateful to the EPSRC for financial support. T.M. is supported by the European Commission and S.M.H. by the Royal Society. This work was supported by the European Union via the Access to Large Scale Facilities Program, Contract No. HPRI-1999-CT-00086.

-
- [1] D. L. Matthews *et al.*, Phys. Rev. Lett. **54**, 110 (1985).
 - [2] S. Suckewer, C. H. Skinner, D. Kim, E. Valeo, D. Voorhees, and A. Wouters, Phys. Rev. Lett. **57**, 1004 (1986).
 - [3] V. N. Shlyaptsev, P. V. Nickles, T. Schlegel, M. P. Kalashnikov, and A. L. Osterheld, Proc. SPIE **2012**, 111 (1993).
 - [4] J. Nilsen, B. J. MacGowan, L. B. Da Silva, and J. C. Moreno, Phys. Rev. A **48**, 4682 (1993).
 - [5] B. E. Lemoff, G. Y. Yin, C. L. Gordon III, C. P. J. Barty, and S. E. Harris, Phys. Rev. Lett. **74**, 1574 (1995).
 - [6] S. Sebban *et al.*, Phys. Rev. Lett. **89**, 253901 (2002).
 - [7] J. J. Rocca, V. Shlyaptsev, F. G. Tomasel, O. D. Cortazar, D. Hartshorn, and J. L. A. Chilla, Phys. Rev. Lett. **73**, 2192 (1994).
 - [8] S. Jackel, R. Burris, J. Grun, A. Ting, C. Manka, K. Evans, and J. Kosakowski, Opt. Lett. **20**, 1086 (1995).
 - [9] F. Dorchie *et al.*, Phys. Rev. Lett. **82**, 4655 (1999).
 - [10] P. Monot, T. Auguste, P. Gibbon, F. Jakober, G. Mainfray, A. Dulieu, M. Louis-Jacquet, G. Malka, and J. L. Miquel, Phys. Rev. Lett. **74**, 2953 (1995).
 - [11] Y. Ehrlich, C. Cohen, A. Zigler, J. Krall, P. Sprangle, and E. Esarey, Phys. Rev. Lett. **77**, 4186 (1996).
 - [12] T. Hosokai, M. Kando, H. Dewa, H. Kotaki, S. Kondo, N. Hasegawa, K. Nakajima, and K. Horioka, Opt. Lett. **25**, 10 (2000).
 - [13] H. M. Milchberg, C. G. Durfee, and T. J. McIlrath, Phys. Rev. Lett. **75**, 2494 (1995).

- [14] P. Volfbeyn, E. Esarey, and W. P. Leemans, *Phys. Plasmas* **6**, 2269 (1999).
- [15] E. W. Gaul, S. P. Le Blanc, A. R. Rundquist, R. Zgadzaj, H. Langhoff, and M. C. Downer, *Appl. Phys. Lett.* **77**, 4112 (2000).
- [16] D. V. Korobkin, C. H. Nam, S. Suckewer, and A. Goltsov, *Phys. Rev. Lett.* **77**, 5206 (1996).
- [17] K. A. Janulewicz, J. J. Rocca, F. Bortolotto, M. P. Kalachnikov, V. N. Shlyaptsev, W. Sandner, and P. V. Nickles, *Phys. Rev. A* **63**, 033803 (2001).
- [18] A. Butler, A. J. Gonsalves, C. M. McKenna, D. J. Spence, S. M. Hooker, S. Sebban, T. Mocek, I. Bettaibi, and B. Cros, *Phys. Rev. Lett.* **91**, 205001 (2003).
- [19] D. J. Spence, A. Butler, and S. M. Hooker, *J. Opt. Soc. Am. B* **20**, 138 (2003).
- [20] N. A. Bobrova, A. A. Esaulov, J. I. Sakai, P. V. Sasorov, D. J. Spence, A. Butler, S. M. Hooker, and S. V. Bulanov, *Phys. Rev. E* **65**, 016407 (2002).
- [21] E. Esarey, P. Sprangle, J. Krall, and A. Ting, *IEEE J. Quantum Electron.* **33**, 1879 (1997).
- [22] D. J. Spence, A. Butler, and S. M. Hooker, *J. Phys. B* **34**, 4103 (2001).
- [23] A. Butler, D. J. Spence, and S. M. Hooker, *Phys. Rev. Lett.* **89**, 185003 (2002).
- [24] S. Augst, D. Strickland, D. D. Meyerhofer, S. L. Chin, and J. H. Eberly, *Phys. Rev. Lett.* **63**, 2212 (1989).
- [25] P. B. Corkum, N. H. Burnett, and F. Brunel, *Phys. Rev. Lett.* **62**, 1259 (2004).
- [26] B. E. Lemoff, C. P. J. Barty, and S. E. Harris, *Opt. Lett.* **19**, 569 (1994).
- [27] S. Sebban *et al.*, *J. Opt. Soc. Am. B* **20**, 195 (2003).
- [28] T. Mocek *et al.*, *Appl. Phys. B: Lasers Opt.* **78**, 939 (2004).
- [29] S. Sebban *et al.*, *Phys. Rev. Lett.* **86**, 3004 (2001).
- [30] M. Pittman, S. Ferre, J. P. Rousseau, L. Notebaert, J. P. Chambaret, and G. Cheriaux, *Appl. Phys. B: Lasers Opt.* **74**, 529 (2002).
- [31] D. J. Spence and S. M. Hooker, *Phys. Rev. E* **63**, 015401 (2001).
- [32] L. Spitzer, Jr., *Physics of Fully Ionized Gases* (Interscience, New York, 1962), Secs. 5.4 and 5.5.
- [33] G. J. Pert, *J. Phys. B* **23**, 619 (1990).
- [34] D. J. Spence and S. M. Hooker, *J. Opt. Soc. Am. B* **17**, 1565 (2000).
- [35] D. J. Spence, A. Butler, and S. M. Hooker, *J. Opt. Soc. Am. B* **20**, 138 (2003).